Cancer Cell, Volume *39*

Supplemental information

Tumor and immune reprogramming during immunotherapy in advanced renal cell carcinoma

Kevin Bi, Meng Xiao He, Ziad Bakouny, Abhay Kanodia, Sara Napolitano, Jingyi Wu, Grace Grimaldi, David A. Braun, Michael S. Cuoco, Angie Mayorga, Laura DelloStritto, Gabrielle Bouchard, John Steinharter, Alok K. Tewari, Natalie I. Vokes, Erin Shannon, Maxine Sun, Jihye Park, Steven L. Chang, Bradley A. McGregor, Rizwan Haq, Thomas Denize, Sabina Signoretti, Jennifer L. Guerriero, Sébastien Vigneau, Orit Rozenblatt-Rosen, Asaf Rotem, Aviv Regev, Toni K. Choueiri, and Eliezer M. Van Allen

Figure S1

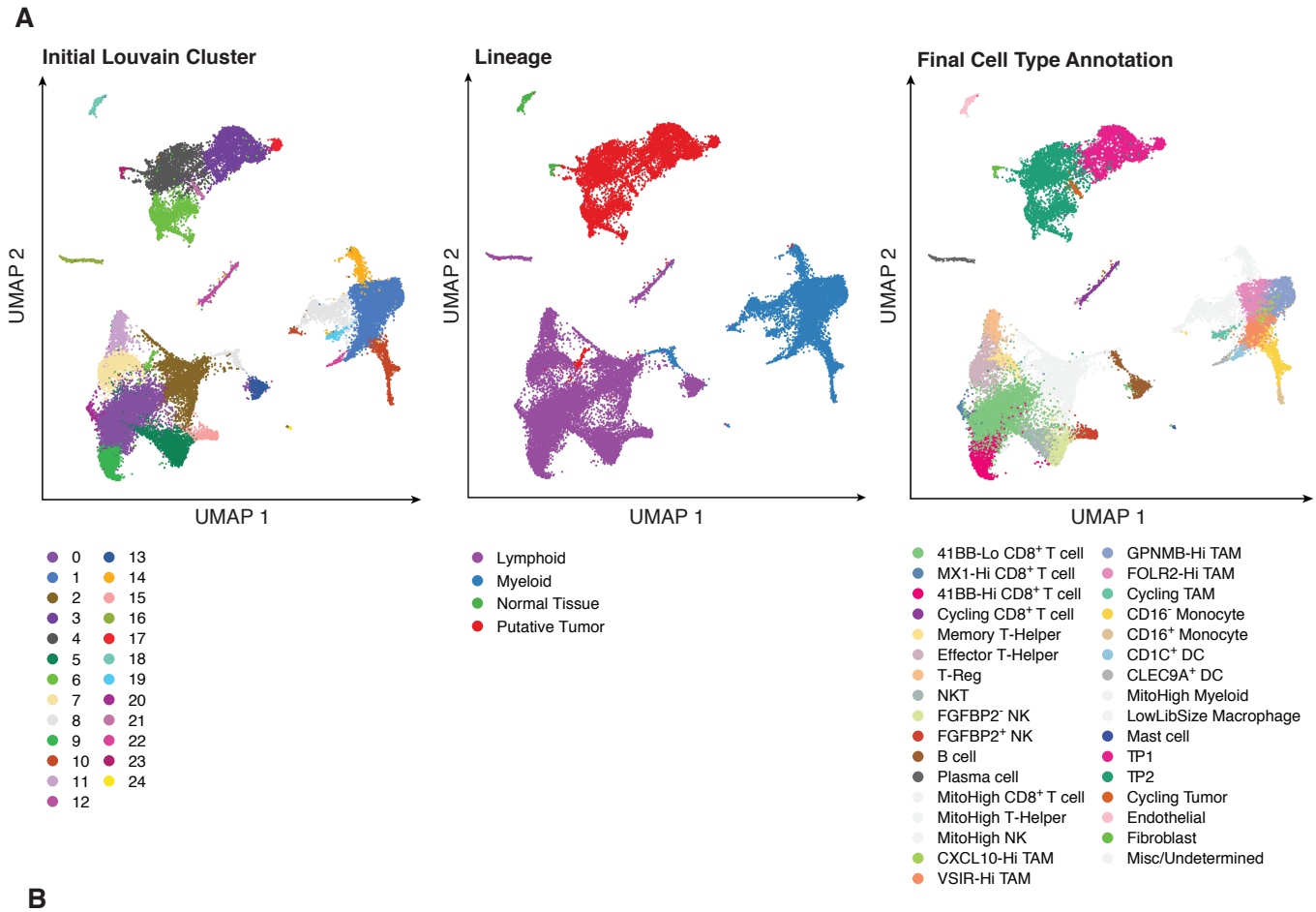
A
Initial Louvain Cluster
Lineage
Final Cell Type Annotation
UMAP 2
UMAP 1
0
1
2
3
4
5
6
7
8
9
10
11
12
13
14
15
16
17
18
19
20
21
22
23
24
Lymphoid
Myeloid
Normal Tissue
Putative Tumor
41BB-Lo CD8+ T cell
MX1-Hi CD8+ T cell
41BB-Hi CD8+ T cell
Cycling CD8+ T cell
Memory T-Helper
Effector T-Helper
T-Reg
NKT
FGFBP2- NK
FGFBP2+ NK
B cell
Plasma cell
MitoHigh CD8+ T cell
MitoHigh T-Helper
MitoHigh NK
CXCL10-Hi TAM
VSIR-Hi TAM
GPNMB-Hi TAM
FOLR2-Hi TAM
Cycling TAM
CD16- Monocyte
CD16+ Monocyte
CD1C+ DC
CLEC9A+ DC
MitoHigh Myeloid
LowLibSize Macrophage
Mast cell
TP1
TP2
Cycling Tumor
Endothelial
Fibroblast
Misc/Undetermined

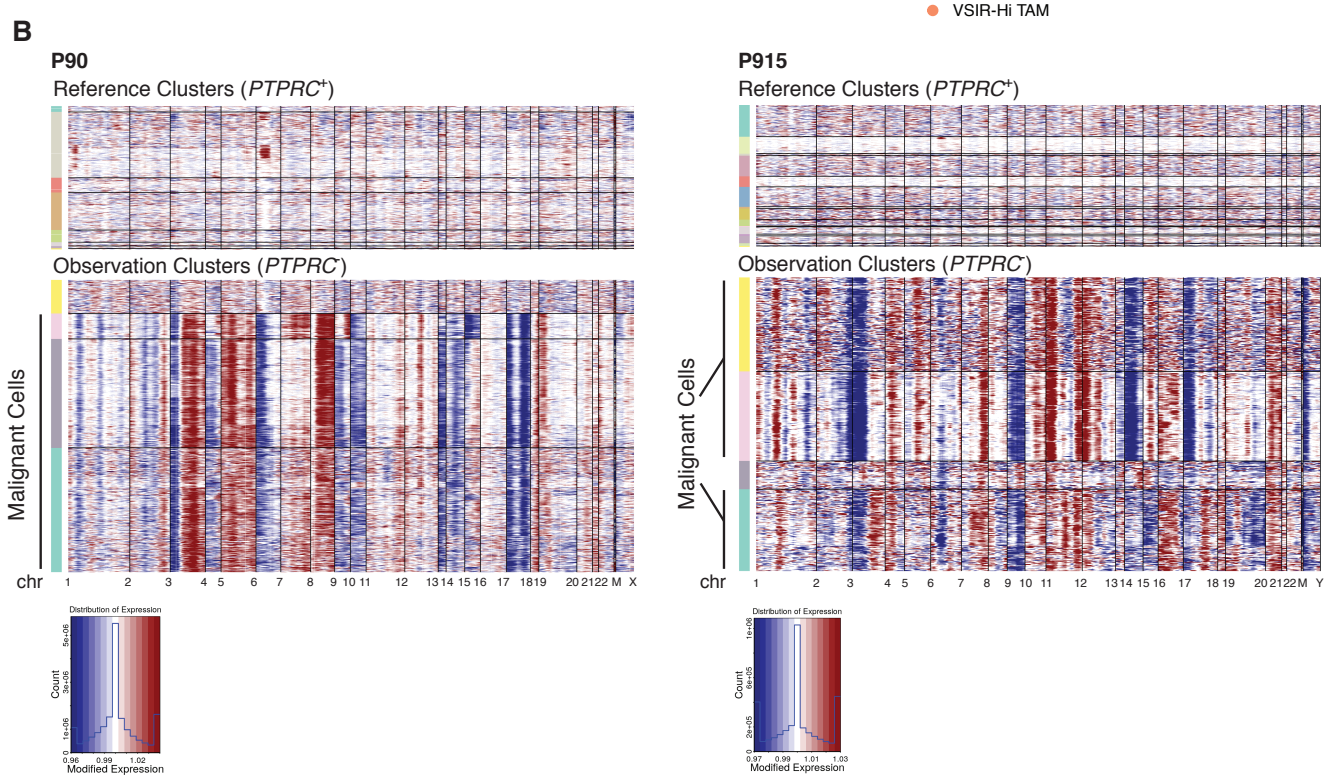
B
P90
Reference Clusters (PTPRC+)
Observation Clusters (PTPRC-)
Malignant Cells
chr
1 2 3 4 5 6 7 8 9 10 11 12 13 14 15 16 17 18 19 20 21 22 M X
Distribution of Expression
Count
Modified Expression
P915
Reference Clusters (PTPRC+)
Observation Clusters (PTPRC-)
Malignant Cells
chr
1 2 3 4 5 6 7 8 9 10 11 12 13 14 15 16 17 18 19 20 21 22 M Y
Distribution of Expression
Count
Modified Expression

Figure S1. Identification of clusters, lineage, and cell subsets. Related to Figure 1.

(A) UMAP of all malignant and non-malignant cells captured across all lesions, colored by initial Louvain cluster (left), lineage (middle), and final cell type annotation following iterative reprojection and clustering within lineages (right).

(B) Heatmaps of inferred CNV for all cells from two representative samples (P90 and P915). Red indicates amplification, while blue indicates deletion. Malignant clusters were identified through broad copy number alteration profiles, including 3p loss characteristic of ccRCC.

Figure S2

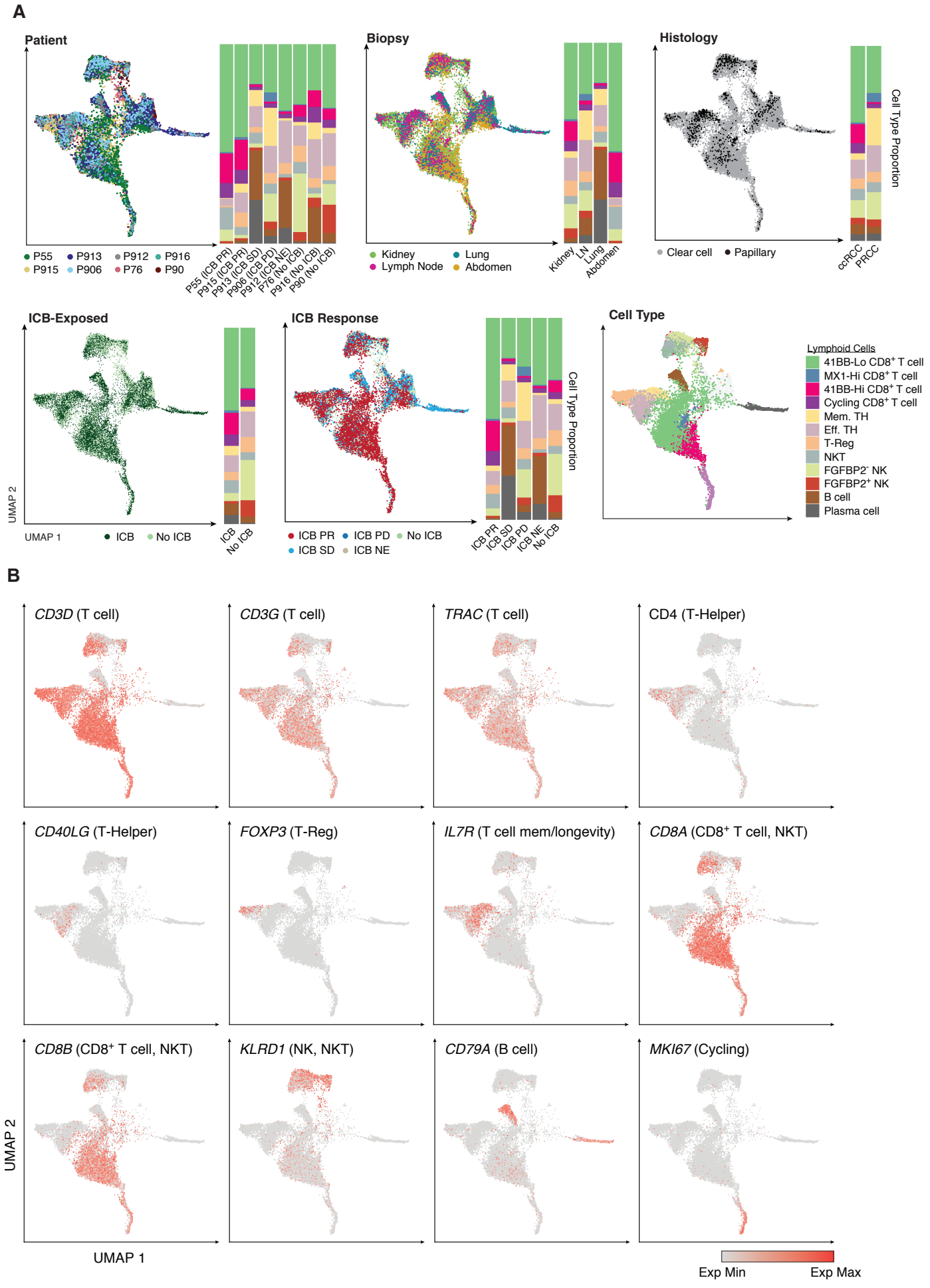
A
Patient
P55
P913
P912
P916
P915
P906
P76
P90
P55 (ICB PR)
P915 (ICB PR)
P913 (ICB SD)
P906 (ICB PD)
P912 (ICB NE)
P76 (No ICB)
P916 (No ICB)
P90 (No ICB)
Biopsy
Kidney
Lung
Lymph Node
Abdomen
Kidney
LN
Lung
Abdomen
Histology
Clear cell
Papillary
ccRCC
PRCC
Cell Type Proportion
ICB-Exposed
UMAP 2
UMAP 1
ICB
No ICB
ICB
No ICB
ICB Response
ICB PR
ICB PD
No ICB
ICB SD
ICB NE
ICB PR
ICB SD
ICB PD
ICB NE
No ICB
Cell Type Proportion
Cell Type
Lymphoid Cells
41BB-Lo CD8+ T cell
MX1-Hi CD8+ T cell
41BB-Hi CD8+ T cell
Cycling CD8+ T cell
Mem. TH
Eff. TH
T-Reg
NKT
FGFBP2- NK
FGFBP2+ NK
B cell
Plasma cell
B
CD3D (T cell)
CD3G (T cell)
TRAC (T cell)
CD4 (T-Helper)
CD40LG (T-Helper)
FOXP3 (T-Reg)
IL7R (T cell mem/longevity)
CD8A (CD8+ T cell, NKT)
CD8B (CD8+ T cell, NKT)
KLRD1 (NK, NKT)
CD79A (B cell)
MKI67 (Cycling)
UMAP 2
UMAP 1
Exp Min
Exp Max

Figure S2

C

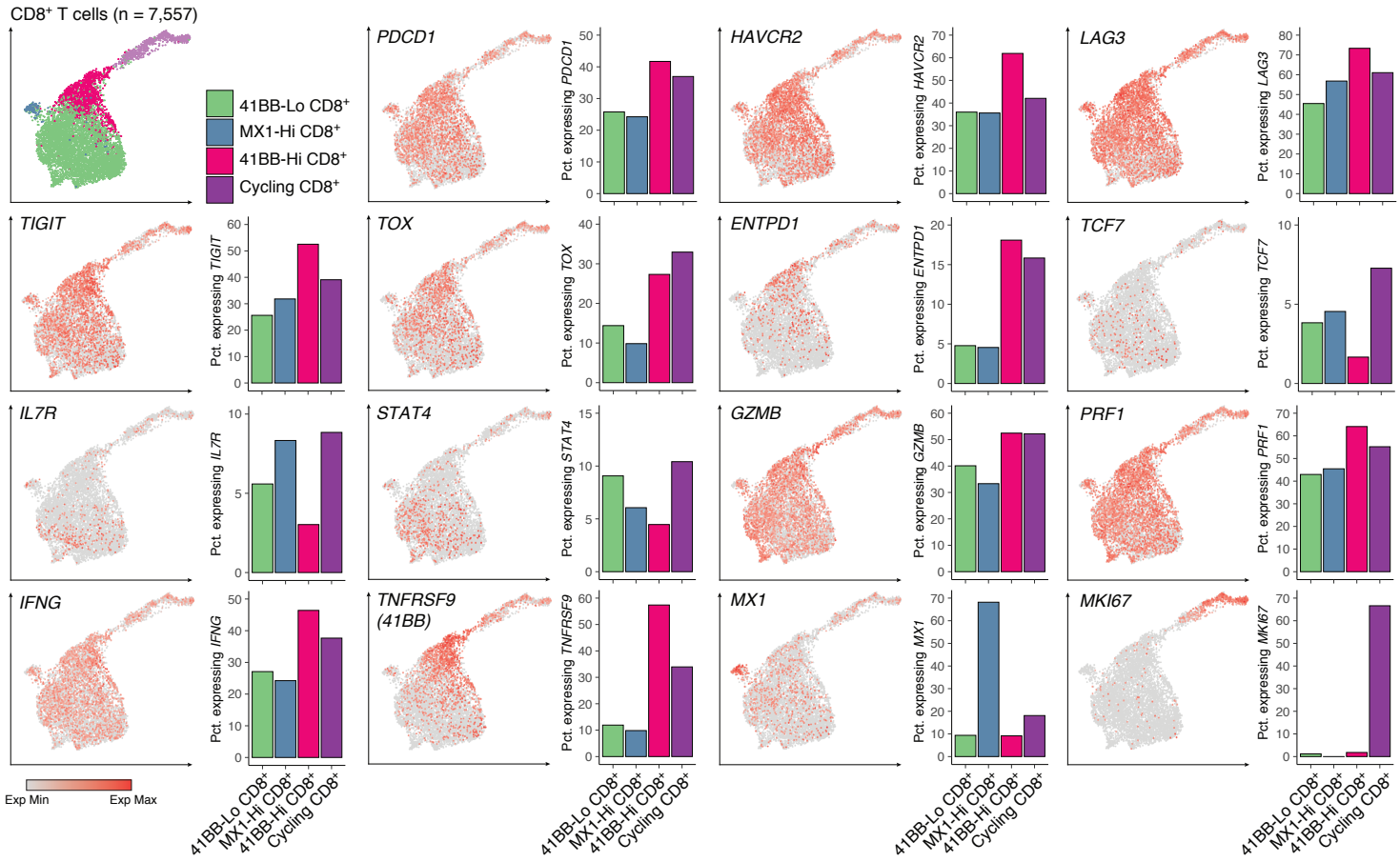
CD8⁺ T cells (n = 7,557)
41BB-Lo CD8⁺
MX1-Hi CD8⁺
41BB-Hi CD8⁺
Cycling CD8⁺
Exp Min
Exp Max
PDCD1
HAVCR2
LAG3
TIGIT
TOX
ENTPD1
TCF7
IL7R
STAT4
GZMB
PRF1
IFNG
TNFRSF9 (41BB)
MX1
MKI67
Pct. expressing PDCD1
Pct. expressing HAVCR2
Pct. expressing LAG3
Pct. expressing TIGIT
Pct. expressing TOX
Pct. expressing ENTPD1
Pct. expressing TCF7
Pct. expressing IL7R
Pct. expressing STAT4
Pct. expressing GZMB
Pct. expressing PRF1
Pct. expressing IFNG
Pct. expressing TNFRSF9
Pct. expressing MX1
Pct. expressing MKI67

Figure S2. Metadata and marker expression for all lymphoid cells and CD8$^+$ T cells. Related to Figure 2.

(A) Visualization of metadata and associated cell type proportions across lymphoid cells.

(B) Expression heatmaps in UMAP projection space of genes encoding cell type and phenotype markers across lymphoid clusters. MitoHigh cells are omitted.

(C) Expression heatmaps in UMAP projection space of genes encoding co-inhibitory receptors, progenitor and terminal exhaustion markers, effector molecules, and cluster-specific genes across CD8$^+$ T cell clusters. Bar plots quantify the percentage of cells in each cluster expressing a given gene.

Figure S3

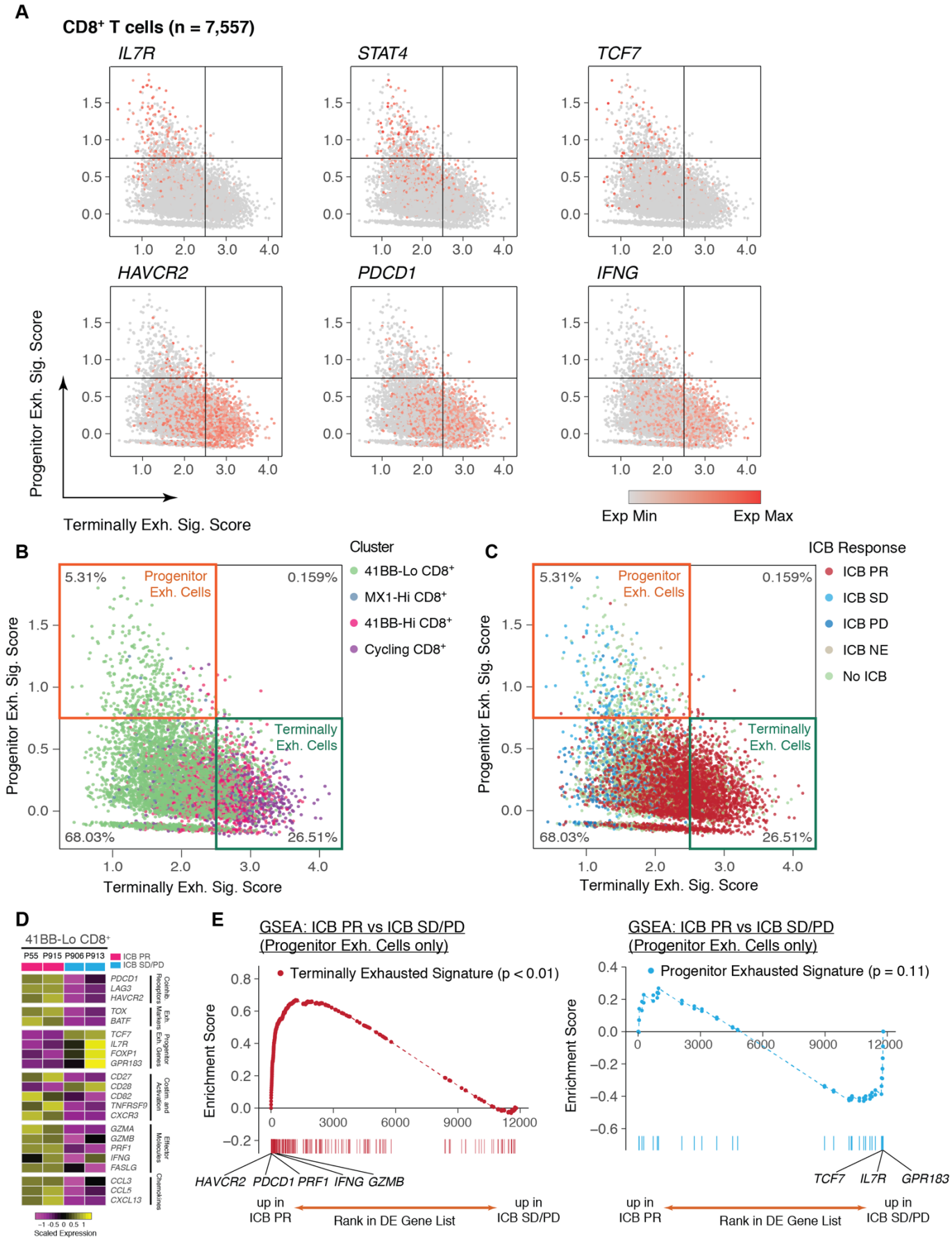
A
CD8+ T cells (n = 7,557)
IL7R
STAT4
TCF7
HAVCR2
PDCD1
IFNG
Progenitor Exh. Sig. Score
Terminally Exh. Sig. Score
Exp Min
Exp Max
B
Cluster
41BB-Lo CD8+
MX1-Hi CD8+
41BB-Hi CD8+
Cycling CD8+
5.31%
Progenitor Exh. Cells
0.159%
Terminally Exh. Cells
68.03%
26.51%
C
ICB Response
ICB PR
ICB SD
ICB PD
ICB NE
No ICB
D
41BB-Lo CD8+
P55 P915 P906 P913
ICB PR
ICB SD/PD
PDCD1
LAG3
HAVCR2
TOX
BATF
TCF7
IL7R
FOXP1
GPR183
CD27
CD28
CD82
TNFRSF9
CXCR3
GZMA
GZMB
PRF1
IFNG
FASLG
CCL3
CCL5
CXCL13
Coinhib. Receptors
Exh. Markers
Progenitor Exh. Genes
Costim. and Activation
Effector Molecules
Chemokines
Scaled Expression
E
GSEA: ICB PR vs ICB SD/PD
(Progenitor Exh. Cells only)
Terminally Exhausted Signature (p < 0.01)
Enrichment Score
HAVCR2 PDCD1 PRF1 IFNG GZMB
up in ICB PR
Rank in DE Gene List
up in ICB SD/PD
GSEA: ICB PR vs ICB SD/PD
(Progenitor Exh. Cells only)
Progenitor Exhausted Signature (p = 0.11)
Enrichment Score
TCF7 IL7R GPR183
up in ICB PR
Rank in DE Gene List
up in ICB SD/PD

Figure S3

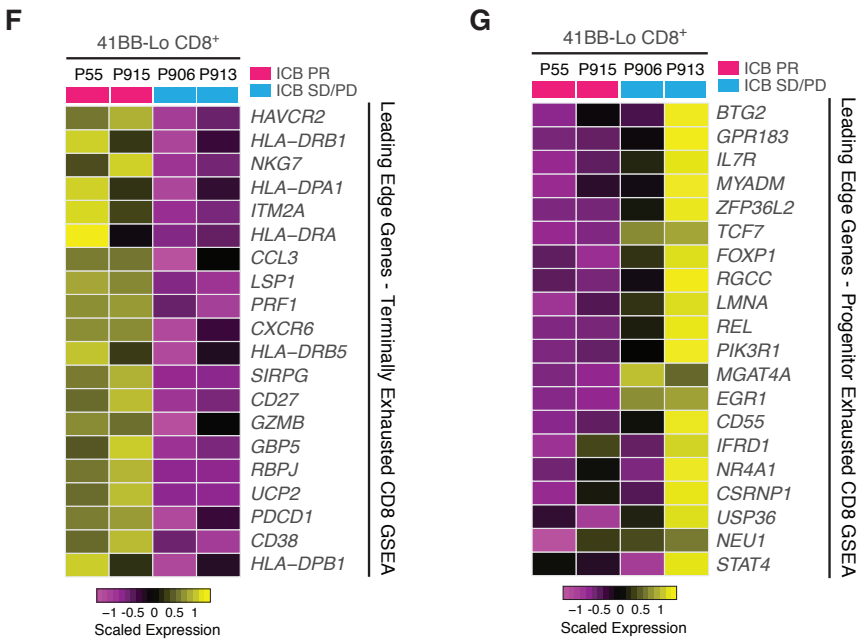
F
41BB-Lo CD8+
P55 P915 P906 P913
ICB PR
ICB SD/PD
HAVCR2
HLA–DRB1
NKG7
HLA–DPA1
ITM2A
HLA–DRA
CCL3
LSP1
PRF1
CXCR6
HLA–DRB5
SIRPG
CD27
GZMB
GBP5
RBPJ
UCP2
PDCD1
CD38
HLA–DPB1
Leading Edge Genes - Terminally Exhausted CD8 GSEA
−1 -0.5 0 0.5 1
Scaled Expression
G
41BB-Lo CD8+
P55 P915 P906 P913
ICB PR
ICB SD/PD
BTG2
GPR183
IL7R
MYADM
ZFP36L2
TCF7
FOXP1
RGCC
LMNA
REL
PIK3R1
MGAT4A
EGR1
CD55
IFRD1
NR4A1
CSRNP1
USP36
NEU1
STAT4
Leading Edge Genes - Progenitor Exhausted CD8 GSEA
−1 -0.5 0 0.5 1
Scaled Expression

Figure S3. Transcriptional characteristics of Progenitor and Terminally Exhausted CD8$^+$ T cells. Related to Figure 2.

(A) Progenitor exhausted signature score versus terminally exhausted signature score for all CD8$^+$ T cells (n = 7,557), points colored by expression of genes of interest.

(B) Progenitor exhausted signature score versus terminally exhausted signature score for all CD8$^+$ T cells (n = 7,557), points colored by CD8$^+$ T cell cluster identity. Progenitor Exhausted and Terminally Exhausted Cells called based on mutually exclusive high/low signature scores. Percentage of total CD8$^+$ T cell is shown for each quadrant.

(C) Progenitor exhausted signature score versus terminally exhausted signature score for all CD8$^+$ T cells (n = 7,557), points colored by ICB response group.

(D) Heatmap of scaled, normalized counts averaged within patients for genes differentially expressed between 4-1BB-Lo CD8$^+$ T cells from ICB PR and ICB SD/PD samples. Effector molecules and co-inhibitory receptors are uniformly upregulated in responding patients, while progenitor exhausted markers, including *TCF7*, are upregulated in non-responding patients.

(E) GSEA of progenitor and terminally exhausted signatures in only Progenitor Exhausted Cells from ICB PR patients compared to ICB SD/PD patients. Key leading edge genes are labeled.

(F) Heatmap of scaled, normalized counts averaged within patients for leading edge genes in GSEA of the terminally exhausted signature in 4-1BB-Lo CD8$^+$ T cells from ICB PR patients compared to ICB SD/PD patients.

(G) Heatmap of scaled, normalized counts averaged within patients for leading edge genes in GSEA of the progenitor exhausted signature in 4-1BB-Lo CD8$^+$ T cells from ICB PR patients compared to ICB SD/PD patients.

Figure S4

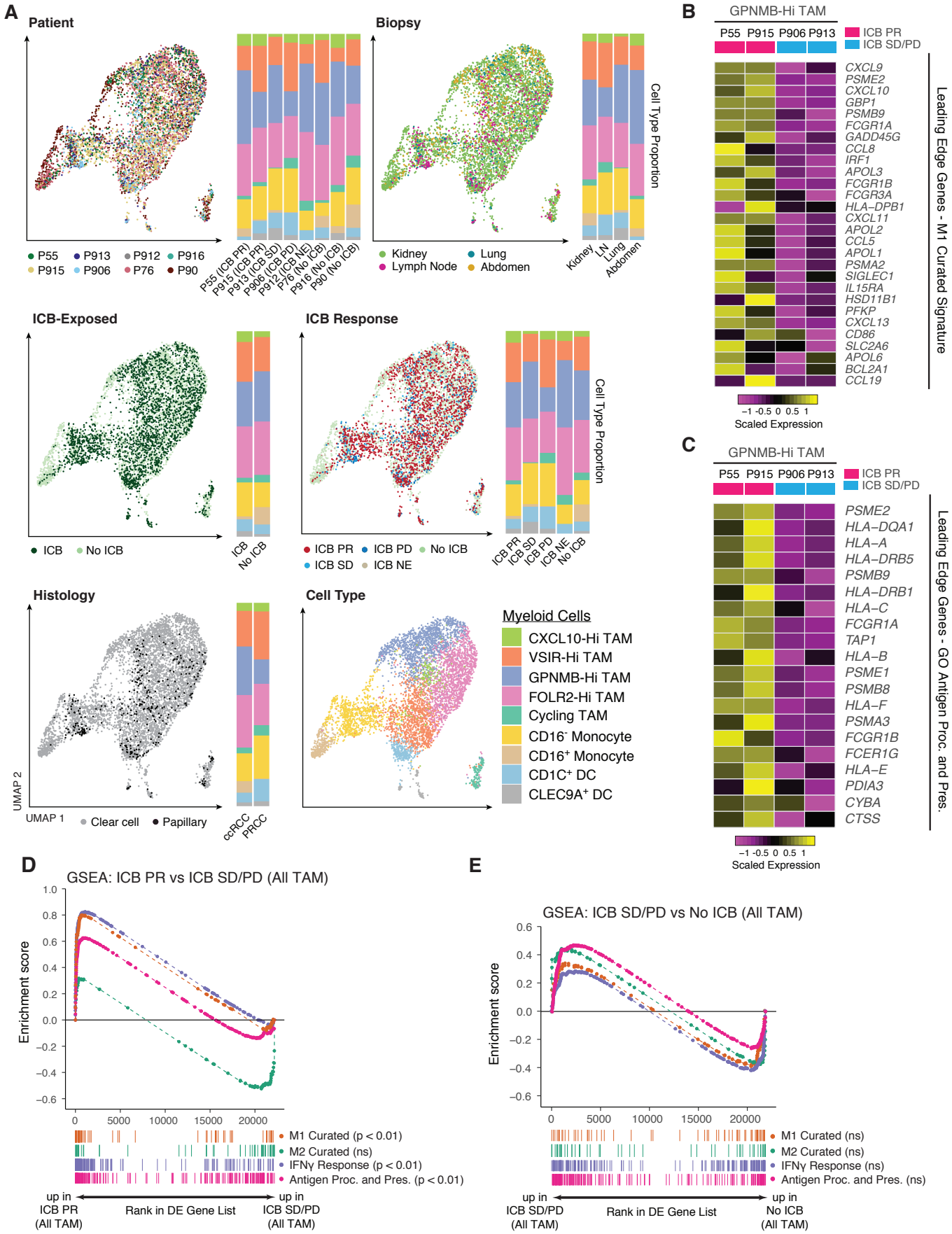
A
Patient
P55
P915
P913
P906
P912
P76
P916
P90
P55 (ICB PR)
P915 (ICB PR)
P913 (ICB SD)
P906 (ICB PD)
P912 (ICB NE)
P76 (No ICB)
P916 (No ICB)
P90 (No ICB)
Biopsy
Kidney
Lymph Node
Lung
Abdomen
Kidney
LN
Lung
Abdomen
Cell Type Proportion
ICB-Exposed
ICB
No ICB
ICB
No ICB
ICB Response
ICB PR
ICB PD
No ICB
ICB SD
ICB NE
ICB PR
ICB SD
ICB PD
ICB NE
No ICB
Cell Type Proportion
Histology
UMAP 2
UMAP 1
Clear cell
Papillary
ccRCC
PRCC
Cell Type
Myeloid Cells
CXCL10-Hi TAM
VSIR-Hi TAM
GPNMB-Hi TAM
FOLR2-Hi TAM
Cycling TAM
CD16- Monocyte
CD16+ Monocyte
CD1C+ DC
CLEC9A+ DC
B
GPNMB-Hi TAM
P55 P915 P906 P913
ICB PR
ICB SD/PD
CXCL9
PSME2
CXCL10
GBP1
PSMB9
FCGR1A
GADD45G
CCL8
IRF1
APOL3
FCGR1B
FCGR3A
HLA–DPB1
CXCL11
APOL2
CCL5
APOL1
PSMA2
SIGLEC1
IL15RA
HSD11B1
PFKP
CXCL13
CD86
SLC2A6
APOL6
BCL2A1
CCL19
Leading Edge Genes - M1 Curated Signature
–1 -0.5 0 0.5 1
Scaled Expression
C
GPNMB-Hi TAM
P55 P915 P906 P913
ICB PR
ICB SD/PD
PSME2
HLA–DQA1
HLA–A
HLA–DRB5
PSMB9
HLA–DRB1
HLA–C
FCGR1A
TAP1
HLA–B
PSME1
PSMB8
HLA–F
PSMA3
FCGR1B
FCER1G
HLA–E
PDIA3
CYBA
CTSS
Leading Edge Genes - GO Antigen Proc. and Pres.
–1 -0.5 0 0.5 1
Scaled Expression
D
GSEA: ICB PR vs ICB SD/PD (All TAM)
Enrichment score
1.0
0.8
0.6
0.4
0.2
0.0
–0.2
–0.4
–0.6
0
5000
10000
15000
20000
M1 Curated (p < 0.01)
M2 Curated (ns)
IFNγ Response (p < 0.01)
Antigen Proc. and Pres. (p < 0.01)
up in ICB PR (All TAM)
Rank in DE Gene List
up in ICB SD/PD (All TAM)
E
GSEA: ICB SD/PD vs No ICB (All TAM)
Enrichment score
0.6
0.4
0.2
0.0
–0.2
–0.4
–0.6
0
5000
10000
15000
20000
M1 Curated (ns)
M2 Curated (ns)
IFNγ Response (ns)
Antigen Proc. and Pres. (ns)
up in ICB SD/PD (All TAM)
Rank in DE Gene List
up in No ICB (All TAM)

Figure S4. Metadata for all myeloid cells and differential gene expression programs in tumor associated macrophages. Related to Figure 3.

(A) Visualization of metadata and associated cell type proportions across myeloid cells.

(B) Heatmap of scaled normalized counts averaged within patients for leading edge genes in GSEA of the M1 Curated signature in GPNMB-Hi TAM from ICB PR patients compared to ICB SD/PD patients.

(C) Heatmap of scaled normalized counts averaged within patients for leading edge genes in GSEA of the GO Antigen Presentation and Processing signature in GPNMB-Hi TAM from ICB PR patients compared to ICB SD/PD patients.

(D) GSEA of M1 Curated, M2 Curated, Hallmark Interferon Gamma Response, and GO Antigen Presentation and Processing via MHC class I signatures in all TAM from ICB PR patients compared to ICB SD/PD patients.

(E) GSEA of M1 Curated, M2 Curated, Hallmark Interferon Gamma Response, and GO Antigen Presentation and Processing via MHC class I signatures in all TAM from ICB SD/PD patients compared to ICB-naive patients.

*ns: not significant

Figure S5

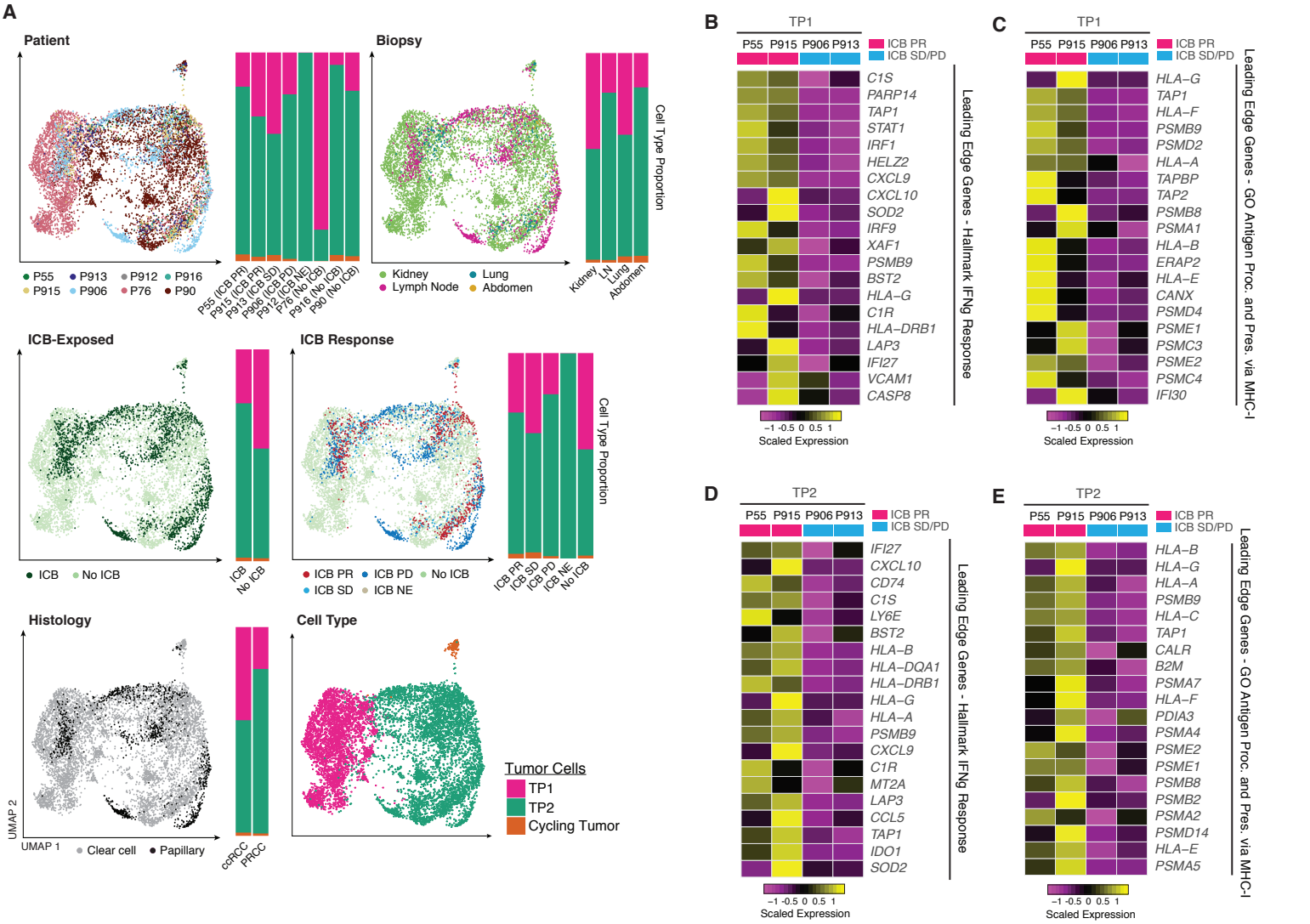
A
Patient
P55 P913 P912 P916
P915 P906 P76 P90
P55 (ICB PR)
P915 (ICB PR)
P913 (ICB SD)
P906 (ICB PD)
P912 (ICB NE)
P76 (No ICB)
P916 (No ICB)
P90 (No ICB)
Biopsy
Kidney Lung
Lymph Node Abdomen
Kidney LN Lung Abdomen
Cell Type Proportion
ICB-Exposed
ICB Response
ICB No ICB
ICB PR ICB PD No ICB
ICB SD ICB NE
ICB PR ICB SD ICB PD ICB NE No ICB
Histology
UMAP 2
UMAP 1
Clear cell Papillary
ccRCC PRCC
Cell Type
Tumor Cells
TP1
TP2
Cycling Tumor
B
TP1
P55 P915 P906 P913
ICB PR
ICB SD/PD
C1S
PARP14
TAP1
STAT1
IRF1
HELZ2
CXCL9
CXCL10
SOD2
IRF9
XAF1
PSMB9
BST2
HLA–G
C1R
HLA–DRB1
LAP3
IFI27
VCAM1
CASP8
Leading Edge Genes - Hallmark IFNg Response
−1 -0.5 0 0.5 1
Scaled Expression
C
TP1
P55 P915 P906 P913
ICB PR
ICB SD/PD
HLA–G
TAP1
HLA–F
PSMB9
PSMD2
HLA–A
TAPBP
TAP2
PSMB8
PSMA1
HLA–B
ERAP2
HLA–E
CANX
PSMD4
PSME1
PSMC3
PSME2
PSMC4
IFI30
Leading Edge Genes - GO Antigen Proc. and Pres. via MHC-I
−1 -0.5 0 0.5 1
Scaled Expression
D
TP2
P55 P915 P906 P913
ICB PR
ICB SD/PD
IFI27
CXCL10
CD74
C1S
LY6E
BST2
HLA–B
HLA–DQA1
HLA–DRB1
HLA–G
HLA–A
PSMB9
CXCL9
C1R
MT2A
LAP3
CCL5
TAP1
IDO1
SOD2
Leading Edge Genes - Hallmark IFNg Response
−1 -0.5 0 0.5 1
Scaled Expression
E
TP2
P55 P915 P906 P913
ICB PR
ICB SD/PD
HLA–B
HLA–G
HLA–A
PSMB9
HLA–C
TAP1
CALR
B2M
PSMA7
HLA–F
PDIA3
PSMA4
PSME2
PSME1
PSMB8
PSMB2
PSMA2
PSMD14
HLA–E
PSMA5
Leading Edge Genes - GO Antigen Proc. and Pres. via MHC-I
−1 -0.5 0 0.5 1
Scaled Expression

Figure S5 **Advanced ccRCC cases only (n = 6)**

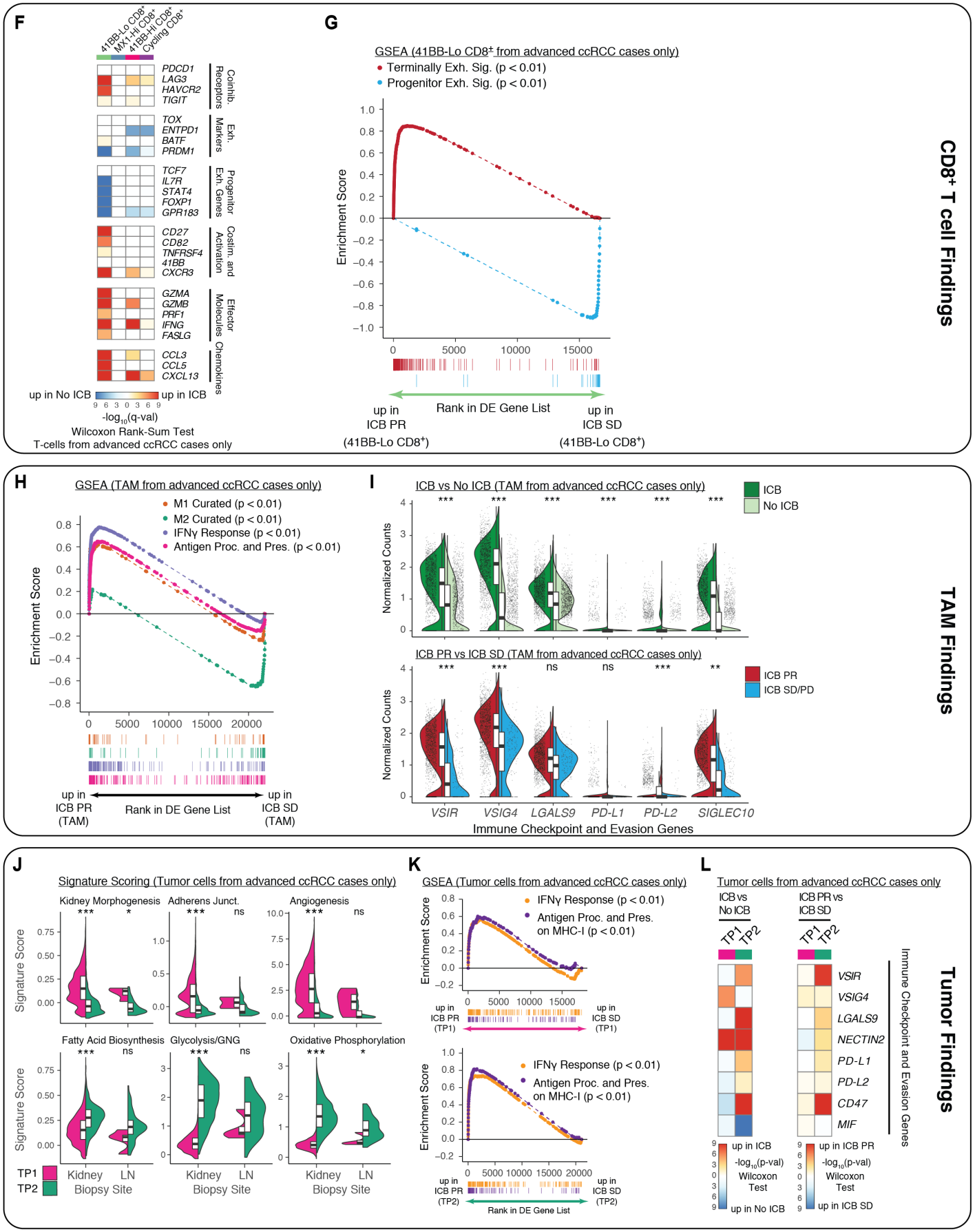

Figure S5. Metadata and differential gene expression programs for tumor cells. Analysis showing reproducibility of main findings in CD8$^+$ T cell, TAM, and tumor compartments when single cell cohort subsetted to include only stage IV lesions of clear cell histology (n = 6). Related to Figure 4.

(A) Visualization of metadata and associated cell type proportions across tumor cells.

(B) Heatmap of scaled normalized counts averaged within patients for leading edge genes in GSEA of the Hallmark Interferon Gamma Response signature in TP1 cells from ICB PR patients compared to ICB SD/PD patients.

(C) Heatmap of scaled normalized counts averaged within patients for leading edge genes in GSEA of the GO Antigen Presentation and Processing via MHC-I signature in TP1 cells from ICB PR patients compared to ICB SD/PD patients.

(D) Heatmap of scaled normalized counts averaged within patients for leading edge genes in GSEA of the Hallmark Interferon Gamma Response signature in TP2 cells from ICB PR patients compared to ICB SD/PD patients.

(E) Heatmap of scaled normalized counts averaged within patients for leading edge genes in GSEA of the GO Antigen Presentation and Processing via MHC-I signature in TP2 cells from ICB PR patients compared to ICB SD/PD patients. (J) Heatmap of differential gene expression q-values (two-sided Wilcoxon rank-sum test with Bonferroni FDR correction) for comparisons of cells within each CD8$^+$ T cell cluster from ICB-exposed vs. ICB-naïve patients (advanced ccRCC cases only).

(F) Heatmap of differential gene expression q-values (two-sided Wilcoxon rank-sum test with Bonferroni FDR correction) for comparisons of cells within each CD8+ T cell cluster from ICB-exposed vs. ICB-naïve patients (advanced ccRCC cases only).

(G) Gene set enrichment analysis (GSEA) of terminally exhausted and progenitor exhausted signatures in 4-1BB-Lo CD8$^+$ T cells from ICB PR compared to ICB SD patients (advanced ccRCC cases only).

(H) GSEA of M1 Curated, M2 Curated, Hallmark Interferon Gamma Response, and GO Antigen Presentation and Processing via MHC class I signatures in all TAM from ICB PR compared to ICB SD patients (advanced ccRCC cases only).

(I) Violin and box plots comparing expression distributions of immune checkpoint and evasion genes between all TAM from ICB-exposed vs ICB-naïve patients (top) and ICB PR vs ICB SD patients (bottom) (advanced

ccRCC cases only). Significance of differential expression (q-value) was determined by two-sided Wilcoxon rank-sum test with Bonferroni FDR correction. Box plots include center line, median; box limits, upper and lower quartiles; whiskers extend at most 1.5× interquartile range past upper and lower quartiles.

(J) Violin and box plots comparing single cell signature score distributions between the two dominant malignant cell clusters, partitioned by biopsy site (advanced ccRCC cases only). Significance of differential signature enrichment (p-value) was determined by two-sided Wilcoxon rank-sum test. Box plots include center line, median; box limits, upper and lower quartiles; whiskers extend at most 1.5× interquartile range past upper and lower quartiles.

(K) GSEA of Hallmark Interferon Gamma Response and GO Antigen Presentation and Processing via MHC class I signatures in TP1 cells from ICB PR patients compared to ICB SD patients (top) and TP2 cells from ICB PR patients compared to ICB SD patients (bottom) (advanced ccRCC cases only).

(L) Heatmap of differential expression q-values (two-sided Wilcoxon rank-sum test with Bonferroni FDR correction) for immune checkpoint and evasion genes in comparisons of cells within each cluster from ICB-exposed vs ICB-naïve patients (left) and ICB PR vs ICB SD patients (right) (advanced ccRCC cases only).

*ns: not significant

Figure S6

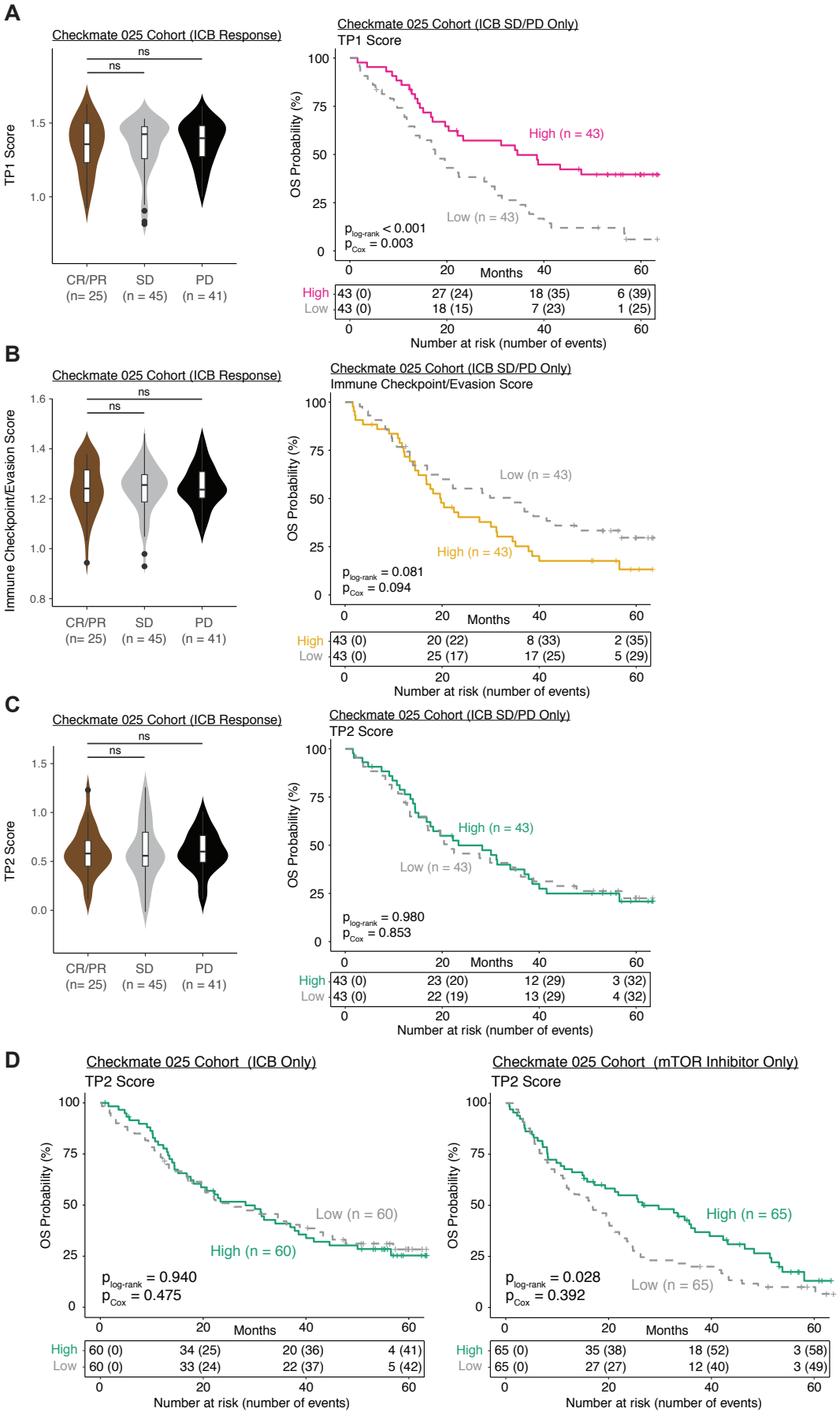
A
Checkmate 025 Cohort (ICB Response)
TP1 Score
ns
ns
CR/PR (n= 25)
SD (n = 45)
PD (n = 41)
Checkmate 025 Cohort (ICB SD/PD Only)
TP1 Score
High (n = 43)
Low (n = 43)
p log-rank < 0.001
p Cox = 0.003
OS Probability (%)
Months
High 43 (0) 27 (24) 18 (35) 6 (39)
Low 43 (0) 18 (15) 7 (23) 1 (25)
Number at risk (number of events)
B
Checkmate 025 Cohort (ICB Response)
Immune Checkpoint/Evasion Score
Checkmate 025 Cohort (ICB SD/PD Only)
Immune Checkpoint/Evasion Score
Low (n = 43)
High (n = 43)
p log-rank = 0.081
p Cox = 0.094
High 43 (0) 20 (22) 8 (33) 2 (35)
Low 43 (0) 25 (17) 17 (25) 5 (29)
C
Checkmate 025 Cohort (ICB Response)
TP2 Score
Checkmate 025 Cohort (ICB SD/PD Only)
TP2 Score
High (n = 43)
Low (n = 43)
p log-rank = 0.980
p Cox = 0.853
High 43 (0) 23 (20) 12 (29) 3 (32)
Low 43 (0) 22 (19) 13 (29) 4 (32)
D
Checkmate 025 Cohort (ICB Only)
TP2 Score
Low (n = 60)
High (n = 60)
p log-rank = 0.940
p Cox = 0.475
High 60 (0) 34 (25) 20 (36) 4 (41)
Low 60 (0) 33 (24) 22 (37) 5 (42)
Checkmate 025 Cohort (mTOR Inhibitor Only)
TP2 Score
High (n = 65)
Low (n = 65)
p log-rank = 0.028
p Cox = 0.392
High 65 (0) 35 (38) 18 (52) 3 (58)
Low 65 (0) 27 (27) 12 (40) 3 (49)

Figure S6

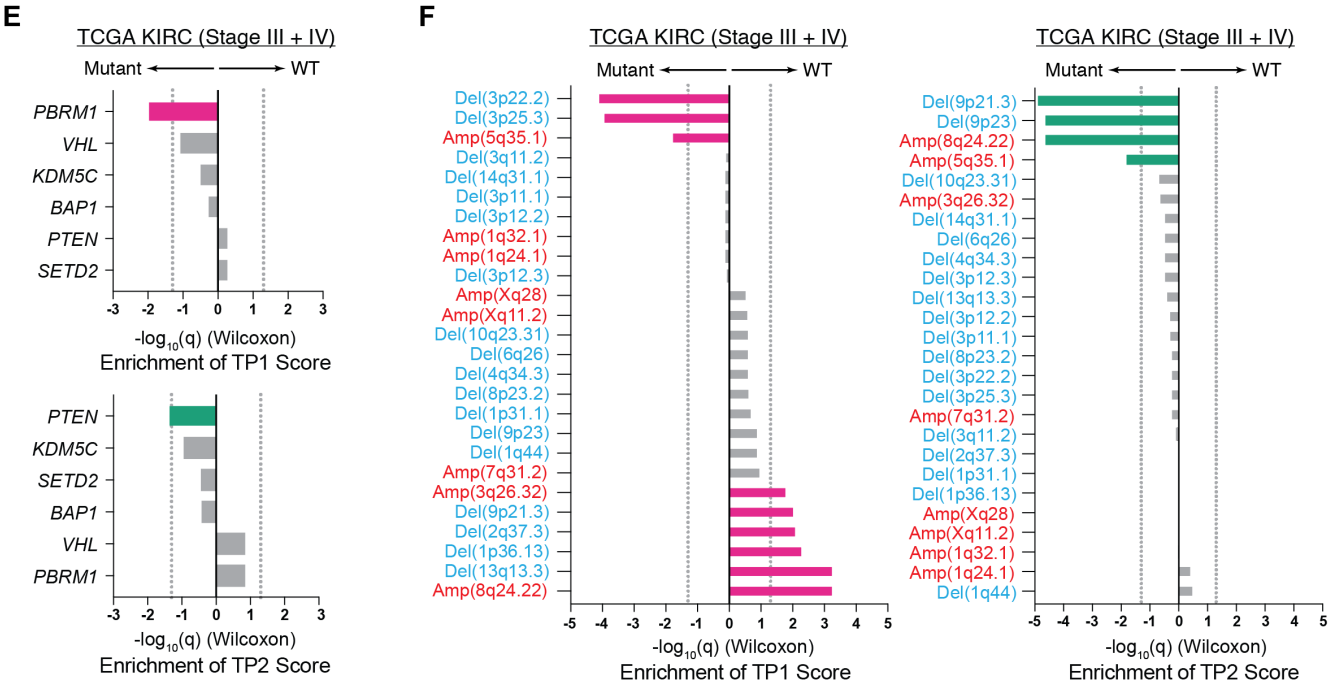
E
TCGA KIRC (Stage III + IV)
Mutant
WT
PBRM1
VHL
KDM5C
BAP1
PTEN
SETD2
-log10(q) (Wilcoxon)
Enrichment of TP1 Score
PTEN
KDM5C
SETD2
BAP1
VHL
PBRM1
-log10(q) (Wilcoxon)
Enrichment of TP2 Score
F
TCGA KIRC (Stage III + IV)
Mutant
WT
Del(3p22.2)
Del(3p25.3)
Amp(5q35.1)
Del(3q11.2)
Del(14q31.1)
Del(3p11.1)
Del(3p12.2)
Amp(1q32.1)
Amp(1q24.1)
Del(3p12.3)
Amp(Xq28)
Amp(Xq11.2)
Del(10q23.31)
Del(6q26)
Del(4q34.3)
Del(8p23.2)
Del(1p31.1)
Del(9p23)
Del(1q44)
Amp(7q31.2)
Amp(3q26.32)
Del(9p21.3)
Del(2q37.3)
Del(1p36.13)
Del(13q13.3)
Amp(8q24.22)
-log10(q) (Wilcoxon)
Enrichment of TP1 Score
TCGA KIRC (Stage III + IV)
Mutant
WT
Del(9p21.3)
Del(9p23)
Amp(8q24.22)
Amp(5q35.1)
Del(10q23.31)
Amp(3q26.32)
Del(14q31.1)
Del(6q26)
Del(4q34.3)
Del(3p12.3)
Del(13q13.3)
Del(3p12.2)
Del(3p11.1)
Del(8p23.2)
Del(3p22.2)
Del(3p25.3)
Amp(7q31.2)
Del(3q11.2)
Del(2q37.3)
Del(1p31.1)
Del(1p36.13)
Amp(Xq28)
Amp(Xq11.2)
Amp(1q32.1)
Amp(1q24.1)
Del(1q44)
-log10(q) (Wilcoxon)
Enrichment of TP2 Score

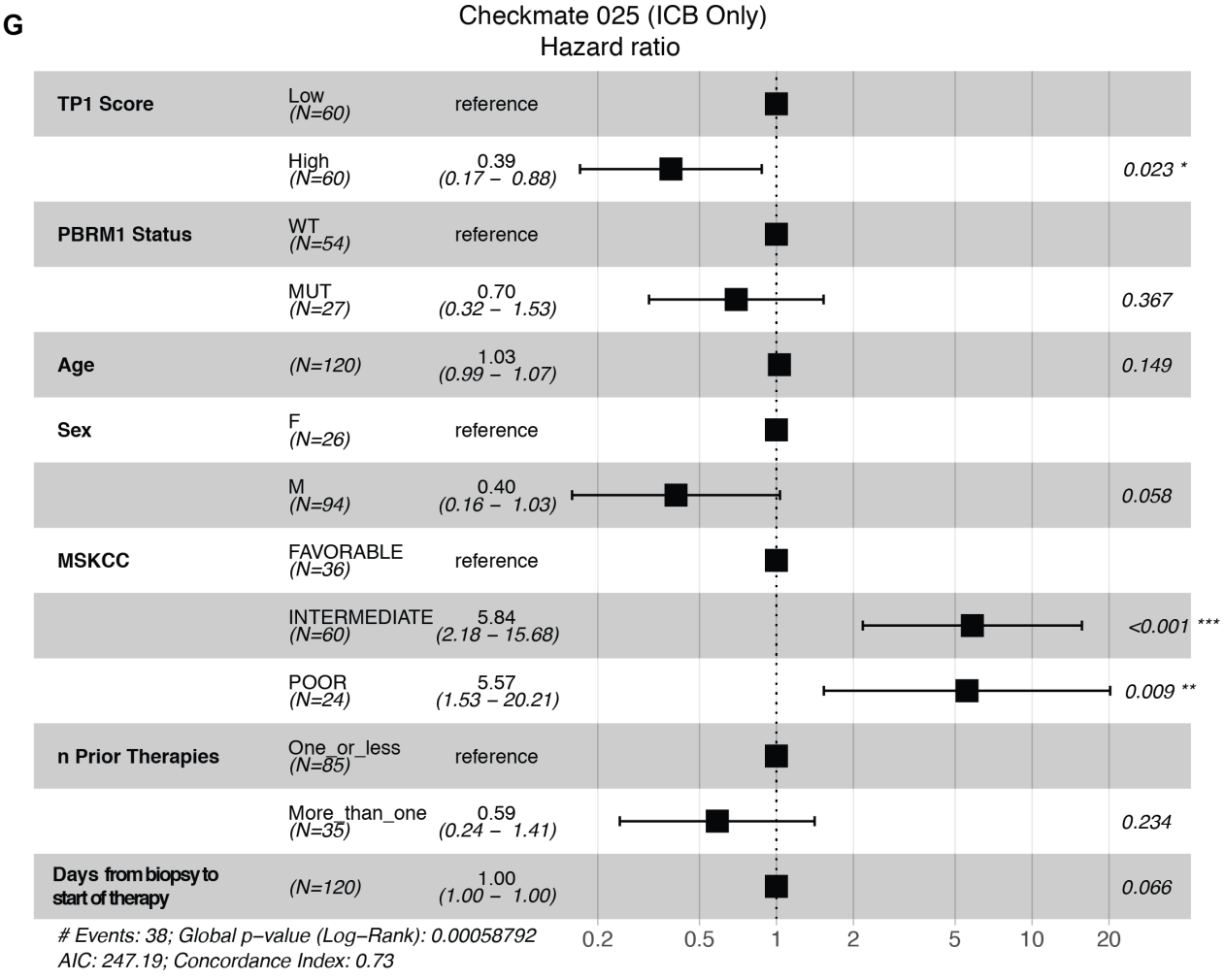
G
Checkmate 025 (ICB Only)
Hazard ratio
TP1 Score
Low (N=60)
reference
High (N=60)
0.39 (0.17 – 0.88)
0.023 *
PBRM1 Status
WT (N=54)
reference
MUT (N=27)
0.70 (0.32 – 1.53)
0.367
Age
(N=120)
1.03 (0.99 – 1.07)
0.149
Sex
F (N=26)
reference
M (N=94)
0.40 (0.16 – 1.03)
0.058
MSKCC
FAVORABLE (N=36)
reference
INTERMEDIATE (N=60)
5.84 (2.18 – 15.68)
<0.001 ***
POOR (N=24)
5.57 (1.53 – 20.21)
0.009 **
n Prior Therapies
One_or_less (N=85)
reference
More_than_one (N=35)
0.59 (0.24 – 1.41)
0.234
Days from biopsy to start of therapy
(N=120)
1.00 (1.00 – 1.00)
0.066
0.2
0.5
1
2
5
10
20
Events: 38; Global p–value (Log–Rank): 0.00058792
AIC: 247.19; Concordance Index: 0.73

Figure S6

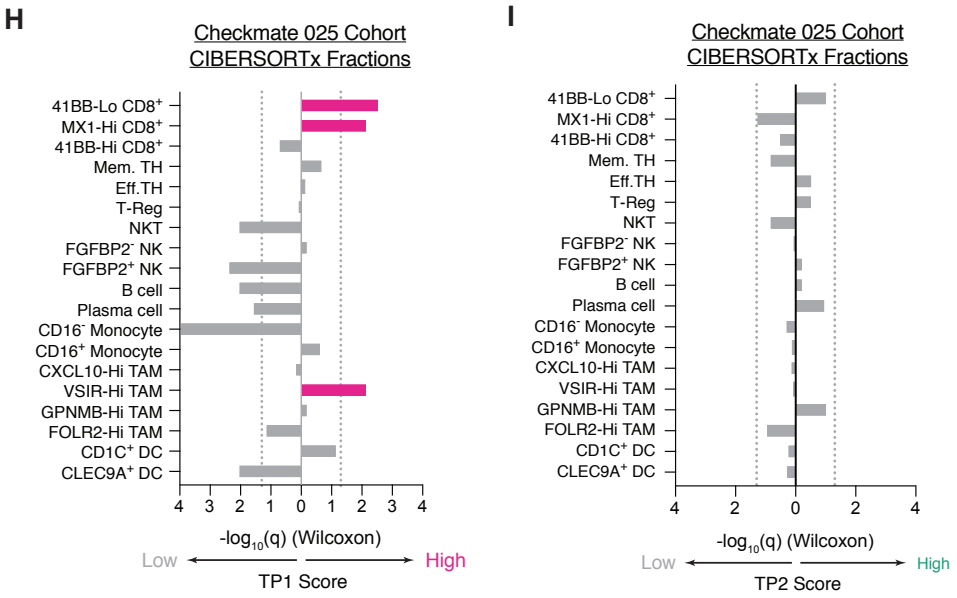
H
Checkmate 025 Cohort
CIBERSORTx Fractions
41BB-Lo CD8+
MX1-Hi CD8+
41BB-Hi CD8+
Mem. TH
Eff.TH
T-Reg
NKT
FGFBP2- NK
FGFBP2+ NK
B cell
Plasma cell
CD16- Monocyte
CD16+ Monocyte
CXCL10-Hi TAM
VSIR-Hi TAM
GPNMB-Hi TAM
FOLR2-Hi TAM
CD1C+ DC
CLEC9A+ DC
4 3 2 1 0 1 2 3 4
-log10(q) (Wilcoxon)
Low
High
TP1 Score
I
Checkmate 025 Cohort
CIBERSORTx Fractions
41BB-Lo CD8+
MX1-Hi CD8+
41BB-Hi CD8+
Mem. TH
Eff.TH
T-Reg
NKT
FGFBP2- NK
FGFBP2+ NK
B cell
Plasma cell
CD16- Monocyte
CD16+ Monocyte
CXCL10-Hi TAM
VSIR-Hi TAM
GPNMB-Hi TAM
FOLR2-Hi TAM
CD1C+ DC
CLEC9A+ DC
4 2 0 2 4
-log10(q) (Wilcoxon)
Low
High
TP2 Score

Figure S6. Extended clinical and mutational analysis of bulk RNA-Seq samples in the Checkmate 025 RCC cohort. Related to Figure 5.

(A) On left, violin and box plots showing distributions of TP1 score within CR/PR, SD, and PD response groups in the ICB arm of the Checkmate 025 RCC cohort. Significance of differential signature enrichment (p-value) was determined by two-sided Wilcoxon rank-sum test. On right, Kaplan-Meier analysis of overall survival (OS) in only the SD and PD response groups of Checkmate 025, with patients separated by high and low TP1 score in bulk RNA-seq. Box plots include center line, median; box limits, upper and lower quartiles; whiskers extend at most 1.5× interquartile range past upper and lower quartiles.

(B) On left, violin and box plots showing distributions of Immune Checkpoint/Evasion score within CR/PR, SD, and PD response groups in the ICB arm of the Checkmate 025 RCC cohort. Significance of differential signature enrichment (p-value) was determined by two-sided Wilcoxon rank-sum test. On right, Kaplan-Meier analysis of overall survival (OS) in only the SD and PD response groups of Checkmate 025, with patients separated by high and low Immune Checkpoint/Evasion score in bulk RNA-seq. Box plots include center line, median; box limits, upper and lower quartiles; whiskers extend at most 1.5× interquartile range past upper and lower quartiles.

(C) On left, violin and box plots showing distributions of TP2 score within CR/PR, SD, and PD response groups in the ICB arm of the Checkmate 025 RCC cohort. Significance of differential signature enrichment (p-value) was determined by two-sided Wilcoxon rank-sum test. On right, Kaplan-Meier analysis of overall survival (OS) in only the SD and PD response groups of Checkmate 025, with patients separated by high and low TP2 score in bulk RNA-seq. Box plots include center line, median; box limits, upper and lower quartiles; whiskers extend at most 1.5× interquartile range past upper and lower quartiles.

(D) Kaplan-Meier analysis of overall survival (OS) in the Checkmate 025 RCC cohort, with patients separated by high and low TP2 score in bulk RNA-seq. $P_{log\text{-}rank}$, log-rank test p-value. P_{Cox}, p-value determined via a multivariate Cox proportional hazard model using TP2 score dichotomized within treatment arm and incorporating age, sex, MSKCC risk group, prior lines of therapy (≤1 or ≥2), and days between biopsy collection and start of trial therapy as covariates.

(E) Bar plots comparing TP1 and TP2 score between mutant and wild-type samples for commonly mutated genes in the TCGA KIRC cohort (Stage III and IV tumors only). Only variants with predicted high impact

Ensembl Sequence Ontology were considered. Significance of differential score enrichment (q-value) determined by two-sided Wilcoxon rank-sum test with Benjamini-Hochberg FDR correction.

(F) Bar plots comparing TP1 and TP2 score between mutant and wild-type samples for common copy number alterations in the TCGA KIRC cohort (Stage III and IV tumors only). Significance of differential score enrichment (q-value) determined by two-sided Wilcoxon rank-sum test with Benjamini-Hochberg FDR correction.

(G) Forest plot showing hazard ratios associated with variables in a multivariate Cox proportional hazard model for OS in the ICB arm of Checkmate 025, incorporating TP1 Score, PBRM1 mutational status, age, sex, MSKCC risk group, prior lines of therapy (≤1 or ≥2), and days between biopsy collection and start of trial therapy as covariates.

(H) Bar plots comparing CIBERSORTx-inferred immune population frequencies between Checkmate 025 RCC tumors with high and low TP1 Tumor Program Scores. CIBERSORTx signature matrix was derived from transcriptional profiles of lymphoid and myeloid subsets captured in our cohort. Significance of differential population frequencies (q-value) determined by two-sided Wilcoxon rank-sum test with Benjamini-Hochberg FDR correction. Gray dotted line corresponds to q = 0.05.

(I) Bar plots comparing CIBERSORTx-inferred immune population frequencies between Checkmate 025 RCC tumors with high and low TP2 Tumor Program Scores. CIBERSORTx signature matrix was derived from transcriptional profiles of lymphoid and myeloid subsets captured in our cohort. Significance of differential population frequencies (q-value) determined by two-sided Wilcoxon rank-sum test with Benjamini-Hochberg FDR correction. Gray dotted line corresponds to q = 0.05.